frontiers in Earth Science

ORIGINAL RESEARCH
published: 20 December 2019
doi: 10.3389/feart.2019.00333

Fatigue Deformation and Energy Change of Single-Joint Sandstone After Freeze-Thaw Cycles and Cyclic Loadings

Yanjun Shen[1,2,3†], Hongwei Yang[4], Long Jin[5], Huan Zhang[4], Gengshe Yang[4] and Jinyuan Zhang[4]*

[1] Geological Research Institute for Coal Green Mining, Xi'an University of Science and Technology, Xi'an, China, [2] College of Geology and Environment, Xi'an University of Science and Technology, Xi'an, China, [3] Shaanxi Provincial Key Laboratory of Geological Support for Coal Green Exploitation, Xi'an University of Science and Technology, Xi'an, China, [4] School of Architecture and Civil Engineering, Xi'an University of Science and Technology, Xi'an, China, [5] CCCC First Highway Consultants Co., Ltd., Xi'an, China

OPEN ACCESS

Edited by:
Yixian Wang,
Hefei University of Technology, China

Reviewed by:
Jun Xian Tan,
Institute of Rock and Soil Mechanics (CAS), China
Chang Q. Sun,
Nanyang Technological University, Singapore
Diego Maria Barbieri,
Norwegian University of Science and Technology, Norway

***Correspondence:**
Yanjun Shen
shenyj@xust.edu.cn

†ORCID:
Yanjun Shen
orcid.org/0000-0001-8109-4819

Specialty section:
This article was submitted to Earth and Planetary Materials, a section of the journal Frontiers in Earth Science

Received: *05 October 2019*
Accepted: *29 November 2019*
Published: *20 December 2019*

Citation:
Shen Y, Yang H, Jin L, Zhang H, Yang G and Zhang J (2019) Fatigue Deformation and Energy Change of Single-Joint Sandstone After Freeze-Thaw Cycles and Cyclic Loadings. Front. Earth Sci. 7:333. doi: 10.3389/feart.2019.00333

In cold regions, saturated fractured rock is prone to crack initiation, extension, and branching along the original fracture end under the effect of freeze-thaw (F-T) cycles and cyclic fatigue loadings. The resulting strength deterioration is accompanied by large amounts of pore growth, which results in localized damage and fracturing along the crack end and even causes overall failure. To study the fatigue damage behaviors of fractured rocks under F-T cycles and cyclic loadings, single-joint quasi-sandstone specimens with joint angles of 45° and 90° were prepared. Subsequently, F-T damage tests with 0, 10, and 20 cycles and cyclic loading tests with different stress levels were performed. The F-T damage features are discussed based on the binarization image of localized damage along the joint ends and their wave velocity variations. It is found that the frost damage of single-joint quasi-sandstone tends toward a strip with localized fatigue characteristics. Moreover, the changes of strain compliance and dissipated energy are studied under the effect of loading-unloading fatigue. Some of the interesting phenomena observed are as follows: (i) during the early stage of cyclic loading, the joint can be compacted; nevertheless, it tends to expand along the fracture direction once it passes the elastic stage, and the irreversible plastic deformation is stable at this stage. (ii) The cracks caused by F-T damage in the 45° single-joint samples deflect along the fracture direction, in contrast to the 90° single-joint specimens. Moreover, the samples with a 45° single joint are more susceptible to original fracture at the early stage of the failure process, which results in a different failure mode from that of the 90° single-joint samples. (iii) The F-T cycles and cyclic loadings have a coupling effect on the single-joint sandstone. The strain compliance and hysteresis energy keep increasing uniformly after the F-T cycles and cyclic loadings.

Keywords: single-joint sandstone, freeze-thaw damage, cyclic loading, fatigue deformation, energy change

INTRODUCTION

The frost-heave effect is an important issue for many environmental and engineering problems in the permafrost region (Pei et al., 2019). During freeze-thaw (F-T) cycles, fractured rocks in cold regions are prone to localized damage and fracture failure along the crack end, which is essentially a problem of fatigue damage by repeated frost-heaving forces and melting (Ruedrich et al., 2011; Jia et al., 2015). Additionally, external cyclic loadings also have an obvious impact on the periodic damage and durability of fractured rocks, which has become a key concern in engineering geological disasters (Gruber et al., 2004; Gruber and Haeberli, 2007; Mu et al., 2018; Yang et al., 2019). Therefore, it is necessary to carry out an experimental study of cumulative fatigue damage and tip fracture evolution of fractured rocks under F-T cycles and periodic loadings, which has practical significance for the understanding and the evaluation of the long-term stability of fractured rock damage in cold regions.

Some interesting research has been carried out on F-T damage and mechanical performance of intact rocks or loess in cold regions (Walder and Hallet, 1985; Krautblatter et al., 2010, 2013; Tan et al., 2011; Pudasaini and Krautblatter, 2014; Shen et al., 2019; Xu et al., 2019). However, few reports exist on the damage mechanism and fracturing process of fractured rocks in cold regions. Matsuoka (1995, 2008) prefabricated fractured granite, studied its fracture expansion process, and proposed that the segregation process of ice in the fissure is the main cause of crack fracture and expansion. Murton et al. (2006) used chalk to explore the action mechanism of segregated ice under F-T cycles in the laboratory. The results showed that macroscopic cracks appeared after the 10th cycle, and the samples completely broke after the 21st cycle. Liu et al. (2015) and Huang et al. (2018) carried out systematic experimental research on the crack frost-heave force of fractured rock in a low-temperature environment and frost-heave crack expansion. The authors argued that the key problems in the study of F-T damage on fractured rocks are as follows: the water transfer mechanism in rocks during the F-T process, the generation and dissipation mechanism of the frost-heave force, and the F-T expansion of fractures.

To explore fatigue deformation and tip fracture of fractured rocks, Yang et al. (2017) carried out cyclic loading tests on prefabricated double-fractured rock and analyzed the initiation, expansion, and penetration process of a crack group under cyclic loadings. Rodríguez et al. (2016) carried out loading-unloading splitting tests on marble disks containing micro-fissures, studied the development and evolution process of micro-cracks, and found that the cracking process is brittle, explosive, and localized. By studying the crack propagation and condensation behavior in rock materials, Lin et al. (2019), Zhao C. et al. (2019), and Cheng et al. (2016) found that the crack opening has a significant impact on the crack initiation stress and path. Yang et al. (2017); Li et al. (2005), and Park and Bobet (2009, 2010) conducted systematic experimental studies on prefabricated fractures of rock model materials and found that new cracks develop and expand steadily along the crack end and incline toward the direction of maximum compressive stress. In addition, many test results showed that the native fissure angle, geometry, and stress condition control the initiation, evolution, and coalescence laws of secondary cracks (Shen et al., 1995; Bobet and Einstein, 1998; Wong and Chau, 1998; Sahouryeh et al., 2002; Wang S. et al., 2019; Wang Y. et al., 2019).

Until now, few experimental studies have comprehensively investigated the F-T damage and loading-unloading fatigue fracture of fractured rocks. However, some previous studies on the fatigue fracture of concrete and rock under the combined action of environmental factors and periodic loadings provide some valuable information (Sun et al., 1999; Jang et al., 2014; Lei et al., 2018; Gao et al., 2019; Tan et al., 2019; Zhao Y. et al., 2019). Therefore, this work used single-joint quasi-sandstone samples with joint angles of 45° and 90°, and the fatigue damage of fractured sandstone was studied experimentally under F-T cycles and periodic loadings. The F-T effect on the degradation of different single-joint sandstones was analyzed by focusing on the wave velocity changes and localized damage binarization images of fractured sandstone samples after different F-T cycles. Moreover, the fatigue deformation process of fractured sandstones was studied by observing the changes of strain compliance and dissipated energy during the loading-unloading process. Under the combined action of F-T cycles and cyclic loadings, different failure modes of fractured sandstone were observed at different angles.

EXPERIMENTAL PROCEDURE

Quasi-Sandstone Sample Preparation

In the past, numerical simulations were typically used to research fractured rock because of sampling difficulties (Wong and Zhang, 2014; Cheng and Zhou, 2015). Park and Bobet (2010), Lee and Jeon (2011); Tang et al. (2001), and Zhou et al. (2014) used gypsum materials or rock-like mix materials to prepare fractured rocks and obtained good test results. In this study, rock-like mix materials are used to produce single-joint sandstones with joint angles of 45° and 90°, which are standard cylindrical samples with a diameter of 50 mm and a height of 100 mm (ASTM C1583–04, 2004). Here, the aggregate is selected to be fine sand screened with a 1.25 mm sieve. The cementing material is high-strength white cement, which is supplemented with common gypsum to enhance its cementing effect. Reduced iron powder with 35-μm-grain is mixed to consider the thermal conductivity of the quasi-sandstone materials; see **Figures 1A,B**. Finally, in order to prefabricate the crack, the iron bar is embedded in a mold; see **Figure 1C**. After the initial setting of the samples, the iron bar is pulled out to form a through crack. The prepared single-joint sandstones can be seen in **Figure 1D**.

Freeze-Thaw Cycle Tests

After the standard samples reach the final setting requirement of 28d, all the samples are saturated using the vacuum pressure saturation device. To ensure that the single crack is completely saturated and not lost, injection of super-cooled water is used to treat the single crack after each F-T cycle; see **Figure 2A**. First, the samples are precooled at a predetermined low temperature.

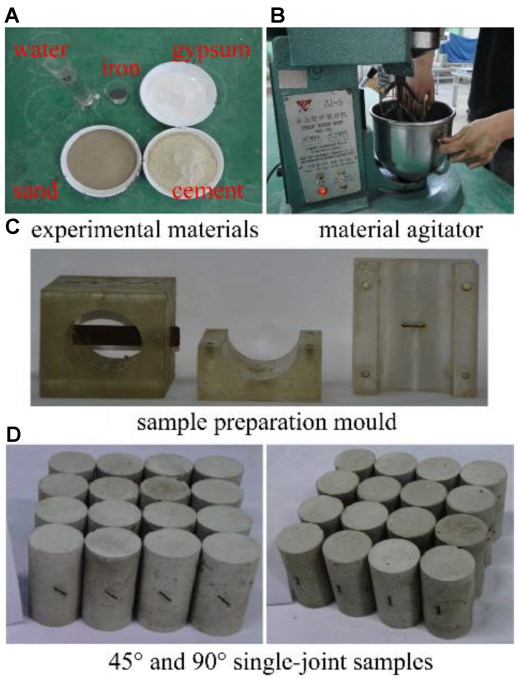

FIGURE 1 | Single-joint sample preparation.

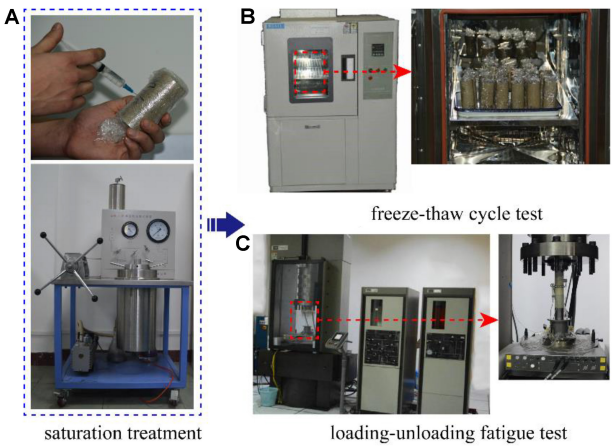

FIGURE 2 | Test equipment and procedure.

When the crack is at the lowest temperature, the samples are wrapped completely in plastic. Then, a syringe is used to inject an amount of water approximately equal to the crack volume. At this time, the water inside the crack rapidly condenses and freezes, and the crack becomes saturated. Subsequently, F-T tests of 0, 10, and 20 cycles are performed on the water-saturated single-joint sandstone samples; see **Figure 2B**. According to the ambient temperature in cold regions, the F-T temperature range is set from −20°C to +20°C, and one cycle lasts 12 h (freezing time: 6 h; thawing time: 6 h). In order to analyze the damage and degradation caused by the F-T cycles on fractured sandstone with different angles, ultrasonic tests and binarization treatment (Particles and Cracks Analysis System, PCAS) (Liu et al., 2011) are performed on the 45° and 90° fractured sandstone after different F-T cycles; see **Table 1**.

Loading-Unloading Fatigue Tests

After 0, 10, and 20 F-T cycles, cyclic loading tests are carried out on the fractured sandstone samples using MTS815 electro-hydraulic test equipment. In order to determine the deformation evolution of the samples during the loading-unloading process accurately, a chain-train extensometer is arranged around the cylindrical samples; see **Figure 2C**. For the fatigue loading test, the sine wave loading mode is adopted for the stress control. First, the upper-limit stress of level I is applied by constant-velocity loading at 0.05 kN/s. Second, the upper-limit stress is unloaded to the corresponding lower-limit stress. The sample undergoes 10 loading-unloading cycles at each stress level. After cyclic loadings at each level, the upper-limit stress is increased by 5% to continue to the next stress level. The test is repeated until the single-joint sandstone is broken. Herein, the upper-limit stress value refers to previous experience from similar tests; the details of the cyclic-loading test scheme are given in **Table 2**.

RESULTS AND DISCUSSION

Localized Damage and Strength Deterioration Analysis

The wave velocity changes of the single-joint rocks under different F-T cycles show that the longitudinal wave velocity is significantly reduced after multiple F-T cycles, and the wave velocities of the 90° single-joint samples are bigger than those

TABLE 1 | Wave velocity changes of single-joint rocks under different F-T cycles.

Single-joint angle	Longitudinal wave velocity (m/s)		
	F-T-0	F-T-10	F-T-20
45°	2146	1942	1642
90°	2277	2145	1994

TABLE 2 | Loading-unloading cyclic test scheme.

F-T cycles (times)	Stress level	Upper-limit stress/Peak strength (%)	Lower-limit stress/Peak strength (%)	Loading-unloading stress amplitude (%)	Cyclic fatigue (times)
0, 10, 20	I	60	30.0	30.0	10
	II	65	32.5	32.5	10
	III	70	35.0	35.0	10
	IV	75	37.5	37.5	10
	V	80	40.0	40.0	10
	VI	85	42.5	42.5	10
	VII	90	45.0	45.0	10
	VIII	95	47.5	47.5	10

of the 45° single-joint samples under the same F-T conditions. For the 45° single-joint samples, the wave velocities sequentially decrease by 204 and 300 m/s after 10 and 20 F-T cycles, respectively. However, that of the 90° single-joint samples only decreases by 132 and 151 m/s after 10 and 20 F-T cycles, correspondingly. This indicates that the samples with a 45° angle are more susceptible to F-T damage. **Figure 3** shows the binarization image of the localized damage process of the 45° and 90° single-joint samples under different F-T cycles. The localized damage effect at the crack end tends to be significant with increasing the number of F-T cycles. The sandstone surface exhibits granule spalling with gradually increasing granule size, and micro-cracks are generated at the crack end. The statistical analysis and calculation show that the localized damage is mainly distributed in a strip along the crack direction with a width of 5d. Remarkably, the cracks caused by F-T damage in the 45° single-joint samples deflect along the fracture direction and accompany a few micro-cracks, in contrast to the 90° single-joint samples. After multiple F-T cycles, the 90° single-joint samples are prone to widening at the lower end, and extended cracks are generated along the fracture direction. These results are consistent with the wave velocity changes and indicate that the interior of saturated single-joint sandstone experiences tensile stress and micro-pore damage under the effect of a repeated frost-heave force, which results in weakened consolidation of mineral particles within the rock.

Frozen rock is a typical heterogeneous granular material composed of solid mineral particles, ideal plastic ice crystals, unfrozen water, and gaseous components (Jia et al., 2019); hence, under negative temperature conditions the volume of rock mineral particles shrinks. However, the volume of pore water and crack water expand because of the water-ice phase transformation, which causes uncoordinated deformation across the particle boundary. It also generates a frost heave force between cracks, internal micro-cracks, and mineral particles that results in broken connections between mineral particles with weaker cementation. At the same time, initiation of local micro-cracks occurs owing to stress concentration at the crack end. When the temperature is higher than the freezing point, the ice melts and the frost-heave force dissipates gradually (Ruedrich et al., 2011; Tan et al., 2018). The freezing and thawing process caused by environmental temperature is equivalent to the loading and unloading fatigue test of fractured rock. When the frost-heave stress reaches the fatigue tensile strength of sandstone material, micro-cracks are initiated, extend, and even break through the material with repeated water-ice phase transformation. In addition, the growth and propagation of each crack provides a bigger space for saturating and freezing-thawing, forming a vicious circle of frost-heaving damage (Shen et al., 2020). As the damage progresses, its extent tends to be directional. The deepening of F-T damage reflects the softening of the fractured rock. According to the development of macroscopic cracks in a localized area, the crack tip can be divided into the following:

(i) a fracture zone that exhibits macroscopic cracks;
(ii) a progressive damage zone with clusters of directional micro-cracks; and
(iii) a systematic damage zone with uniformly distributed stress.

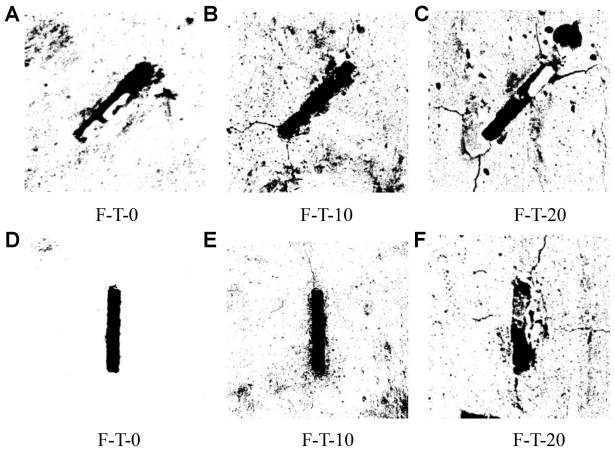

FIGURE 3 | Binarization image of localized damage under different F-T cycles.

Figure 4 shows the stress-strain curves of the fractured sandstone samples under cyclic loadings after 0, 10, and 20 F-T cycles, in which the axial and volumetric strain are positive and the circumferential strain is negative. By comparing and analyzing the evolution laws governing the relationship between the stress and axial strain, circumferential strain, and volumetric strain of the 45° and 90° single-joint samples during loading-unloading under different F-T cycles, the following main features can be obtained:

(1) With increasing number of F-T cycles, the corresponding fatigue fracture strength of the 45° and 90° single-joint sandstone samples gradually decreases during the loading-unloading process. Additionally, the fatigue fracture strength of the 90° single-joint samples is bigger than that of the 45° single-joint samples under the same F-T conditions. These results are consistent with the above analysis and indicate that the F-T cycles cause obvious internal cumulative damage to the fractured sandstone, which aggravates the strain softening process of the fractured sandstone.
(2) As the number of F-T cycles increases, the hysteresis loop curve of the relationship between the loading-unloading stress and the axial strain shows an obvious expansion, which reflects that the plastic damage strain inside the sample gradually increases with increasing F-T cycles. Its external appearance is characterized by the initiation and extension of macroscopic cracks along the crack end that accompany secondary wing cracks as shown in **Figure 3**. Moreover, there is systematic damage caused by frost-heaving inside the sample, which is refle cted by wave velocity variations.
(3) With increasing number of F-T cycles, the curves of loading-unloading stress and volumetric strain exhibit

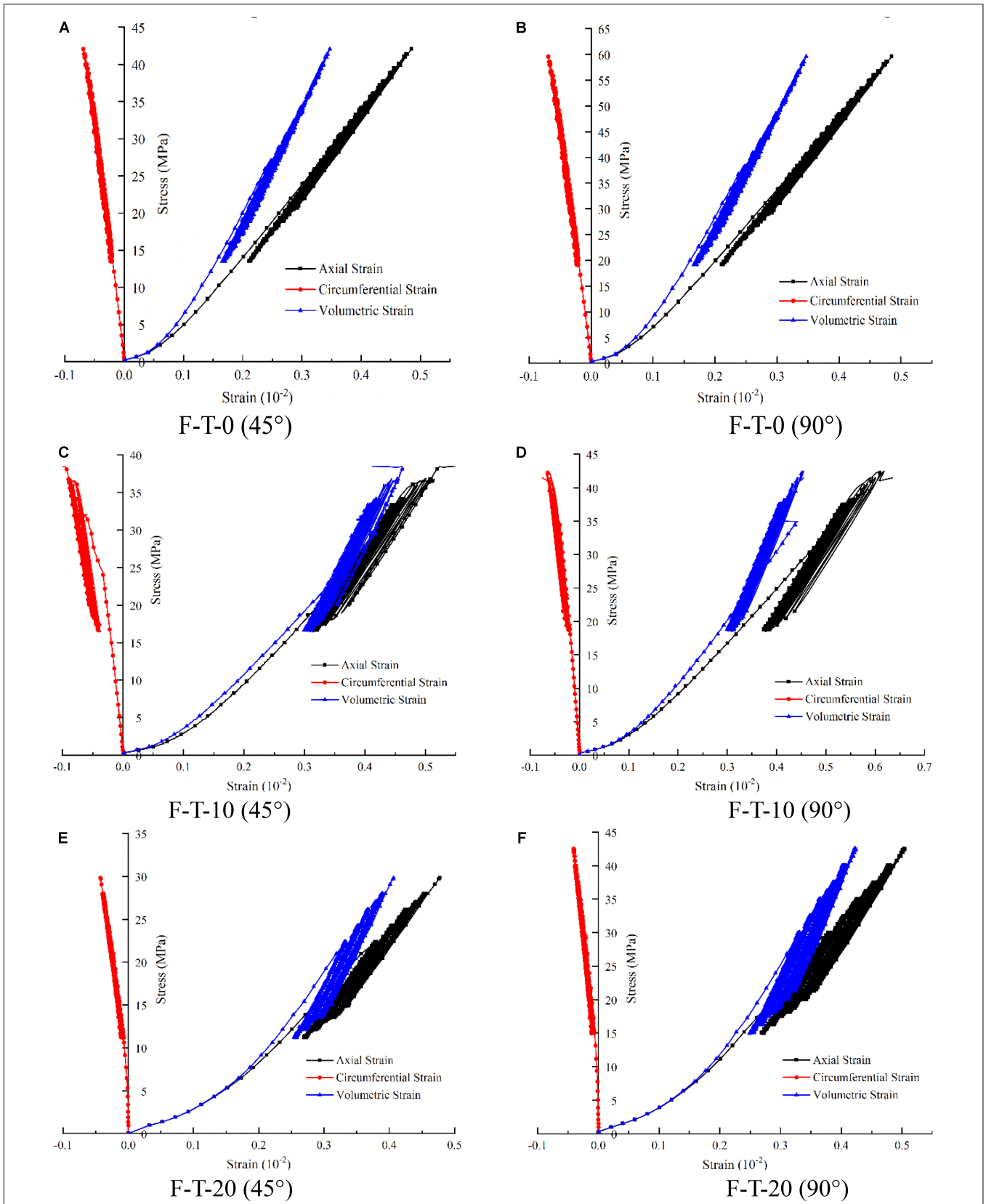

FIGURE 4 | The stress-strain curves of fractured sandstone under different F-T cycles.

obvious hysteresis, and the hysteresis loop curve expands partly after the F-T cycles. This indicates that after F-T damage the interior of the sample is loose and its cementation and structure are weakened. When subjected to a load, volumetric strain is generated rapidly. During the loading-unloading process, the overall volume shrinkage rate tends to be significant, which is positively correlated with the F-T cycles. In addition, it can be observed in **Figure 4** that no significant difference exists between the loading-unloading stress and circumferential strain curves under different F-T cycles.

(4) Compared with the 90° single-joint samples, the slope of the hysteresis loop curves of the 45° single-joint samples is always slightly lower. That means that the strain of the 45° single-joint sandstone is more sensitive to the stress changes in the loading-unloading process. This indicates that the 45° single-joint sandstone is more affected by F-T damage and its plastic deformation is more prominent. This also confirms the results of the binarization image analysis.

Deformation and Fracture Characteristics Analysis

As mentioned previously, there are significant differences between the variation laws of the hysteresis loop curves obtained under different F-T conditions. Liu et al. (2018) and Tutuncu et al. (2002a,b) conducted an experimental study on the deformation law of porous granular sedimentary rocks under uniaxial cyclic stress and found that the characteristics of the stress-strain hysteresis loop are closely related to the stress condition and the strain amplitude. To analyze the deformation characteristics of fractured sandstone during variable-amplitude cyclic loadings, Qiu et al. (2012) used the concept of strain compliance $\Delta\dot{\varepsilon}$, which is the ratio of the strain increment caused by axial compression to the corresponding stress amplitude during cyclic loadings at each stress level.

$$\Delta\dot{\varepsilon}_{(a,c,v)} = \frac{\Delta\varepsilon_{(a,c,v)}}{\Delta\sigma} \tag{1}$$

Here, $\Delta\varepsilon_a$, $\Delta\varepsilon_c$, and $\Delta\varepsilon_v$ are the axial, circumferential, and volumetric strain increments, respectively.

The strain compliance $\Delta\dot{\varepsilon}$ is a physical quantity representing the change rate of the deformation increment in each direction under the action of loading-unloading axial compression. It can effectively reflect the effect of cyclic loading variation on the deformation of fractured sandstone. Moreover, it represents the response speed of the internal structure of sandstone to the stress mode and change process (Shen et al., 2018). **Figure 5** shows the variation rules of axial, circumferential, and volumetric strain compliance under different loading-unloading stress levels. The figure demonstrates that:

(1) After being subjected to 0, 10, and 20 F-T cycles, the 45° single-joint sandstone samples were destroyed at the loading-unloading stress levels VII, V, and V, respectively. The corresponding 90° single-joint sandstone samples were destroyed at the loading-unloading stress levels VIII, VI, and V, respectively. This shows that the F-T cycle has a significant effect on the degradation of the fatigue strength of the fractured sandstone samples. After the F-T cycles, micro-cracks develop and expand gradually at the end of the original fracture. Meanwhile, the number of internal pores of the sample increase, the structure becomes loose, and the resistance to cyclic fatigue loadings decreases.

(2) The absolute values of axial, circumferential, and volumetric strain compliance are all relatively large at stress level I. Subsequently, a trend of an initial decrease and a subsequent uniform increase appears. This indicates that the sample has experienced three development stages under the cyclic loadings: a compaction phase, an elastic phase, and a plastic phase. At the initial stage of repeated loading-unloading, the structure and mechanical properties of the rock can be optimized, such as reduction of the original pores, closure of cracks, and enhancement of inter-component occlusion. As shown in **Figure 5**, larger deformation occurs at stress level I of the cyclic loading process, and the recoverable deformation is limited during the unloading process, so the strain compliance is relatively large. Then, the sample gradually transits to the elastic stage, and the deformation can be recovered during the loading and unloading process. The strain increment decreases and generally reaches the valley value at stress level III. Finally, with the increase of the stress level of the cyclic loadings, the sample enters the plastic stage, and each loading and unloading cycle makes the damage develop on the original basis. The axial, circumferential, and volumetric strain compliance gradually increase with the cyclic loadings. This is characterized by the occurrence of micro-cracks around the micro-pores in the sandstone due to stress concentration, initiation and expansion of the original closed cracks accompanied by secondary wing cracks, overall cracking through along the original crack direction, and final failure.

(3) The more F-T cycles the fractured sandstone samples are subjected to, the greater strain compliance and the more significant the increasing or decreasing trend of the strain compliance. Sandstone is susceptible to F-T damage in the saturated state because of its porous structure. The composition and structure of internal mineral particles are degraded by the frost-heaving force, which reduces the compactness of the material and the adhesion between particles and enhances its brittleness. Under the cyclic loadings, the strain is increased, the compaction phase is prolonged, the elastic phase is shortened, and the variation law is significantly enhanced.

(4) All the absolute values of strain compliance (axial, circumferential, and volumetric strain compliance) of the 45° single-joint sandstone are bigger than those of the 90° single-joint sandstone samples. Further, the variation trend and slope of the strain compliance of the 45° single-joint sandstone are more steep. This indicates that the compaction stage and plastic deformation of slant fractured sandstone are more obvious under the combined action of F-T cycles and periodic loadings compared with a fracture parallel to the loading direction, which is

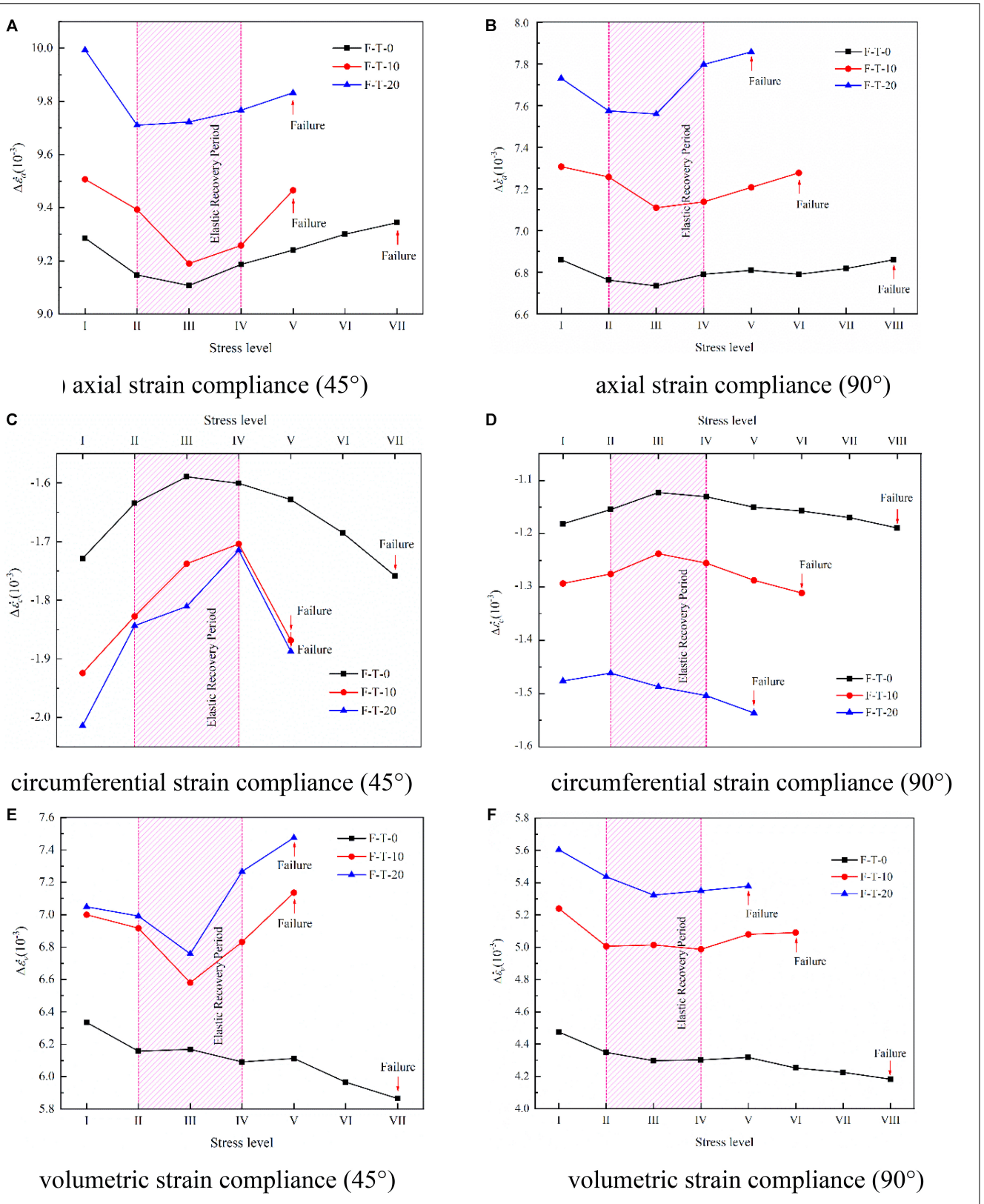

FIGURE 5 | Relationship between the rate of strain compliance and the loading-unloading stress level of fractured sandstones under different F-T cycles.

characterized by increased pores, more cracks, weakened particle bonding, and brittle material.

After F-T damage, the 45° and 90° single-joint samples experienced different deformation phases under cyclic loadings and broke at a certain stress level. The 45° and 90° single-joint sandstone samples exhibited two completely different fracture morphologies; see **Figure 6**. The 45° single-joint sample shows typical tensile-shearing failure along the original fracture; two main cracks appeared along the load direction at both ends of the original fracture, creating severe crushing and particle spalling around the fracture. However, crushing areas occur at both ends of the 90° single-joint sandstone sample and larger particles are spalled. There is only one main crack along the 90° single-joint, which is parallel to the load direction. It is the typical splitting failure along the original fracture end. This is the result of cumulative damage under the F-T cycles and cyclic loadings, which can be explained by the concept of the "minimum resistance area."

For the 45° single-joint sandstone samples, the minimum resistance area can be seen in **Figures 7a1,a2**. Because the projected area of the 45° single-joint is not considered as the resistance area, the stress in the middle of the sample is different from that on both sides; see **Figure 7a3**. Under axial fatigue loadings, the 45° single-joint sample is subjected to tensile shearing failure and forms cracks; as shown in **Figure 7a4**. Subsequently, the original fracture is compacted and tends to close under the loading-unloading process, and crushing and particle spalling occur around the original fracture owing to the stress concentration and the localized weak area caused by the F-T cycles. Finally, the main failure mode formed, as shown in **Figure 7a5**. **Figure 7a6** illustrates the failure morphologies of the 45° single-joint sandstone samples; the main cracks are deflected owing to localized damage and wing cracks are caused by the F-T cycles.

The projected area of the 90° single-joint is very small, and the minimum resistance area is close to the projected area of the cylindrical sample section, as shown in **Figures 7b1,b2**. Under axial fatigue loadings, the early stage of the failure process of the sandstone sample is equivalent to the loading state of intact cylindrical sandstone; see **Figure 7b3**. Therefore, there is crushing of bigger areas and spalling on both ends of the sample; see **Figure 7b4**. Subsequently, vertical splitting failure occurs in the sandstone at the original fracture ends, and a crack forms along the fracture direction; see **Figure 7b5**. **Figure 7b6** depicts the failure morphologies of the 90° single-joint sandstone samples.

Energy Evolution Analysis

The elastic-plastic deformation failure of fractured rock is essentially a process of energy dissipation. The law of energy evolution in the process of fatigue failure can reflect the essential characteristics of the deformation, damage, and failure of fractured rock. Under the action of uniaxial periodic loadings, part of the total energy absorbed by the rock becomes elastic-strain energy and the remaining energy is

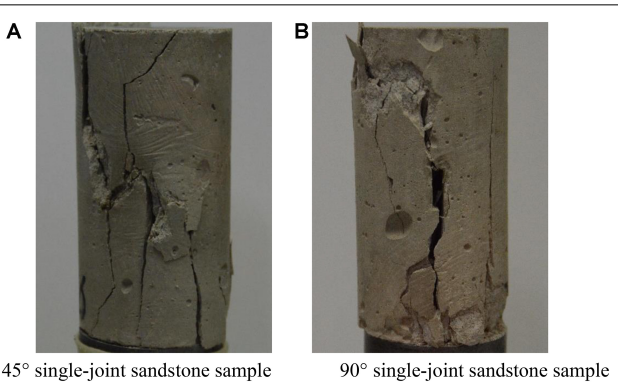

FIGURE 6 | Comparison of fracture morphologies.

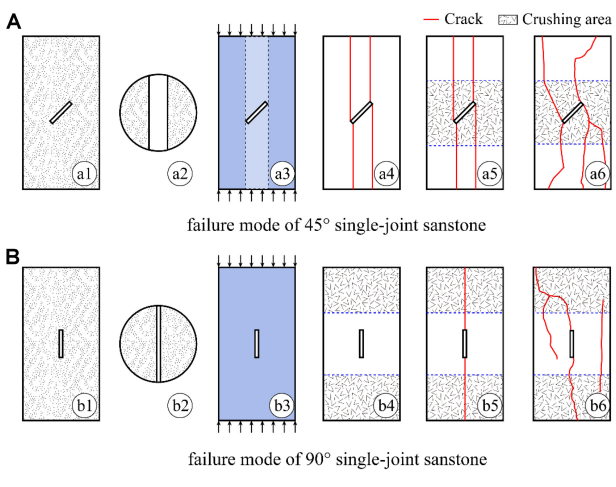

FIGURE 7 | Failure modes of the 45° and 90° single-joint sandstone samples.

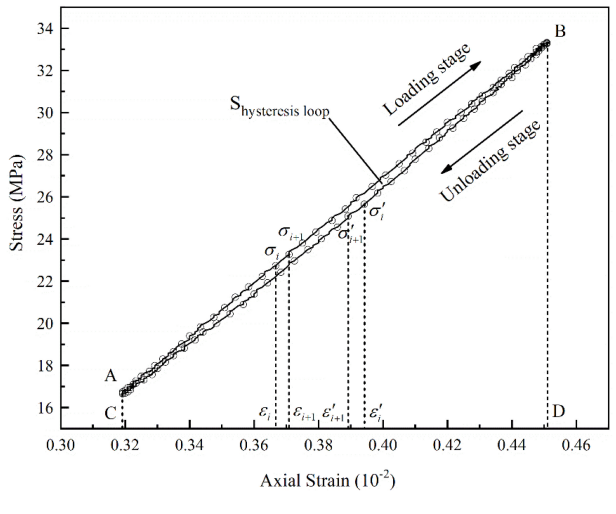

FIGURE 8 | The 7th hysteresis loop at stress level I under 10 F-T cycles.

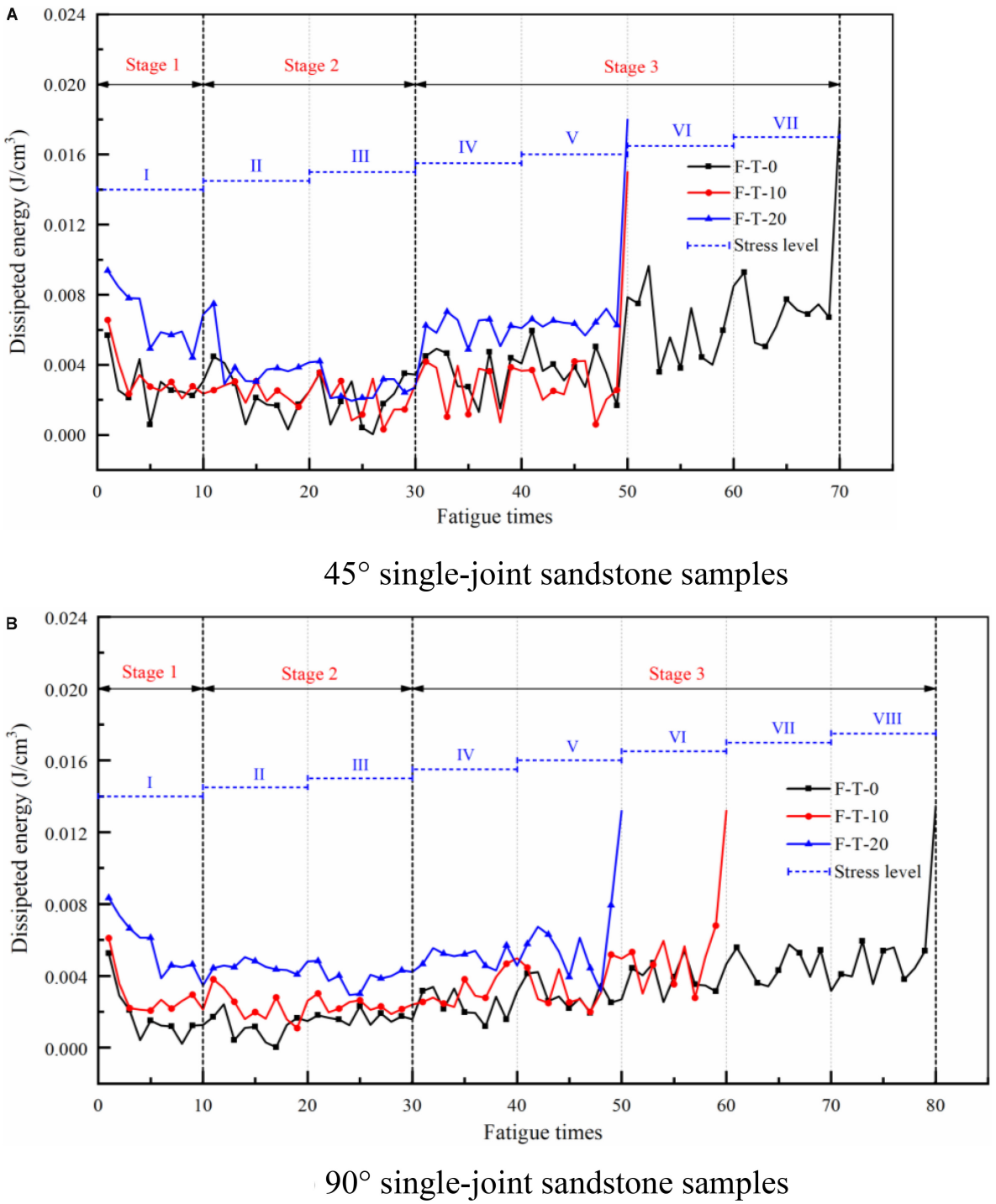

FIGURE 9 | Evolution law of dissipated energy per unit volume with fatigue times under different F-T cycles.

dissipated in the form of heat and radiant energy (dissipated energy). Bagde and Petroš (2005, 2009) studied the influence of strain amplitude and frequency on the fatigue and energy characteristics of sandstone under cyclic loadings. Rodríguez et al. (2016) analyzed the evolution law of crack expansion under different loading-unloading paths from the perspective of energy. According to the relationship between the area of the hysteresis loop of the stress-strain curve obtained under cyclic loadings and the dissipated energy (Xiao et al., 2010), the area enclosed by the axial stress-strain curve and the strain in a cyclic loading stage

is the unit volume energy E_v. Further, the area enclosed by the axial stress-strain curve and the strain at the unloading stage is the elastic deformation energy per unit volume E_e, and the area of the hysteresis loop in each cycle is the dissipated energy per unit volume E_c. In this study, the 7th hysteresis loop at stress level I of cyclic loading under 10 F-T cycles is considered as an example to describe the calculation of the area of the hysteresis loop; see **Figure 8**.

$$E_c = E_v - E_e = \frac{1}{2}\left[\sum(\sigma_i + \sigma_{i+1}) \cdot (\varepsilon_{i+1} - \varepsilon_i) - \sum(\sigma'_i + \sigma'_{i+1}) \cdot (\varepsilon'_i - \varepsilon'_{i+1})\right] \quad (2)$$

Here, σ_i and σ_{i+1} are the axial stresses at points i and i+1, respectively, on the axial loading curve, in MPa; ε_i and ε_{i+1} are the corresponding axial strains; σ'_i and σ'_{i+1} are the axial stresses at points i and i+1, respectively, on the axial unloading curve, in MPa; ε'_i and ε'_{i+1} are the corresponding axial strains.

Figure 9 shows the evolution law of the dissipated energy per unit volume with fatigue cycles during loading and unloading. In the loading-unloading fatigue test, the dissipated energy is mainly the plastic deformation energy required for crack initiation, propagation, and penetration; it also includes the plastic deformation energy that causes irreversible damage inside the rock. For the 45° and 90° single-joint sandstone samples tested under different F-T cycles, with increasing loading-unloading stress level, the variation rules of the dissipated energy per unit volume are different, which can be mainly summarized by the following four points:

(1) The unit volume energy and the elastic-strain energy per unit volume generally increase in a step-like manner with increasing stress level during loading and unloading. The more F-T cycles are subjected to, the smaller the unit volume energy and the strain energy per unit volume are. As the axial dissipated energy per unit volume (that is, the area of the hysteresis loop) increases with increasing F-T cycles, the change range is relatively small compared with the case of no F-T cycles. This shows that the elastic-strain energy of fractured sandstone can be reduced by the F-T damage and dissipated owing to deformation; that is, the dissipated energy is unrecoverable.

(2) The evolution of dissipated energy per unit volume of sandstone under 10 and 20 F-T cycles is mainly observed in stages 1, 2, and 3. In stage 1, which is the initial stage of cyclic loadings, the energy input by the system is dissipated owing to unrecoverable deformation, such as pore compaction and crack closure in the sample, so the dissipated energy per unit volume is relatively large. In stage 2, the dissipated energy gradually decreases with increasing fatigue loading cycles. The sample density increases, the elastic-strain energy increases, and the dissipated energy continues to oscillate around the lower value. Later, in stage 3, the stress level is larger, the internal structure of sandstone is gradually damaged under complex stress conditions, and more cracks are activated and integrated. All these continue irreversible damage, and dissipated energy increases gradually in this process. When the cumulative crack density reaches a certain threshold, the fractured sandstone material fails. The evolution process is consistent with the strain compliance variation law shown in **Figure 5**. The results show that it is a simple and effective way for quantitatively analyzing the energy evolution and deformation characteristics of samples under loading-unloading fatigue tests by using the area of the hysteresis loop.

(3) The sandstone sample that did not undergo any F-T cycles is a standard room-temperature test sample with larger particle inter-granular intensity, prominent anisotropic features, and severe deformation. The dissipated energy increases gradually owing to the diverse and irregular deformation, and the amplitude of oscillation increases until failure. Moreover, after fatigue failure, the sandstone structure is observed to be relatively broken, and the local characteristics of the 10 and 20 F-T cycle samples after failure are obvious.

(4) Compared with the variation laws of the dissipated energy per unit volume of the 45° and 90° single-joint sandstone samples under different F-T cycles, the values of dissipated energy per unit volume of the 90° single-joint sandstone are slightly smaller, and the change trends are gentler, which is consistent with the results of the strain compliance analysis. However, with increasing loading-unloading stress level, the dissipated energy per unit volume in stage 2 does not increase and decrease visibly. This also indicates that the internal damage and development of cracks in the sandstone samples at this stage converge.

CONCLUSION

(1) The frost-heaving damage of the fractured sandstone caused by the F-T cycles is a tip fatigue failure problem, showing typical localized damage characteristics. Crack development gradually moves from the fracture zone to the progressive-damage zone, accompanied by unrecoverable system damage. This forms a vicious cycle of secondary crack extension and material strength degradation.

(2) The cyclic loadings strengthen the mechanical properties of fractured sandstone in the early densification stage. With increasing loading-unloading stress level and stress amplitude, the cracks are activated again and expand along the fracture direction after the elastic stage, and the irreversible plastic deformation is enhanced continuously. The corresponding hysteretic loop becomes round, and the strain compliance and dissipated energy per unit volume increase gradually.

(3) Under the combined action of the F-T cycles and cyclic loadings, the fatigue damage characteristics of fractured sandstone are not only related to the stress conditions but are also closely related to the F-T cycles. The greater number of F-T cycles are subjected to, the more significant the fatigue damage characteristics are, and the greater the

corresponding strain compliance and dissipated energy are. In addition, the F-T damage and the fatigue failure of cyclic loading have a superposition effect. The localized damage and systematic damage caused by the former can promote the development of fatigue damage.

(4) The failure mode of the 45° single-joint sandstone is typical tensile-shearing failure, which consists of initial fracture and subsequent crushing. However, the failure mode of the 90° single-joint sandstone is typical splitting failure along the original fracture end, which is the opposite process. In addition, the 45° single-joint sandstone is more susceptible to original fracture and results in localized damage under F-T cycles and cyclic loadings.

DATA AVAILABILITY STATEMENT

All datasets generated for this study are included in the article.

AUTHOR CONTRIBUTIONS

YS, LJ, and HZ conceived and designed the experiments. HY and JZ performed the experiments. YS and HY analyzed the data. YS and GY contributed funding supports. HY wrote the manuscript. YS revised the English language of this manuscript.

FUNDING

This research was funded by the National Natural Science Foundation of China (Grant No. 41772333), the National Natural Science Foundation of Shaanxi Province, China (Grant No. 2018JQ5124), the New-Star Talents Promotion Project of Science and Technology of Shaanxi Province, China (Grant No. 2019KJXX049), and the Foundation of Key Laboratory of Western Mineral Resources and Geological Engineering of Ministry of Education, Chang'an University (Grant No. 300102268503).

REFERENCES

ASTM C1583–04, (2004). *Standard Test Method for Tensile Strength of Concrete Surfaces and the Bond Strength or Tensile Strength of Concrete Repair and Overlay Materials by Direct Tension (pull–off method)*. West Conshohocken, PA: ASTM International, doi: 10.1520/C1583-04

Bagde, M. N., and Petroš, V. (2005). Fatigue properties of intact sandstone samples subjected to dynamic uniaxial cyclical loading. *Int. J. Rock Mech. a Min. Sci.* 42, 237–250. doi: 10.1016/j.ijrmms.2004.08.008

Bagde, M. N., and Petroš, V. (2009). Fatigue and dynamic energy behaviour of rock subjected to cyclical loading. *Int. J. Rock Mech. Min. Sci.* 46, 200–209. doi: 10.1016/j.ijrmms.2008.05.002

Bobet, A., and Einstein, H. H. (1998). Fracture coalescence in rock-type materials under uniaxial and biaxial compression. *Int. J. Rock Mech. Min. Sci.* 35, 863–888. doi: 10.1016/S0148-9062(98)00005-9

Cheng, H., and Zhou, X. (2015). A multi-dimensional space method for dynamic cracks problems using implicit time scheme in the framework of the extended finite element method. *Int. J. Damage Mech.* 24, 859–890. doi: 10.1177/1056789514555149

Cheng, H., Zhou, X., Zhu, J., and Qian, Q. (2016). The effects of crack openings on crack initiation, propagation and coalescence behavior in rock-like materials under uniaxial compression. *Rock Mech. Rock Eng.* 49, 3481–3494. doi: 10.1007/s00603-016-0998-9

Gao, X., Liu, C., Tan, Y., Yang, N., Qiao, Y., Hu, Y., et al. (2019). Determination of fracture properties of concrete using size and boundary effect models. *Appl. Sci* 9:1337. doi: 10.3390/app9071337

Gruber, S., and Haeberli, W. (2007). Permafrost in steep bedrock slopes and its temperatures-related destabilization following climate change. *J. Geophys. Res. Earth Surf.* 112:F02S18. doi: 10.1029/2006JF000547

Gruber, S., Hoelzle, M., and Haeberli, W. (2004). Permafrost thaw and destabilization of Alpine rock walls in the hot summer of 2003. *Geophys. Res. Lett.* 31:L13504

Huang, S. B., Liu, Q. S., Chen, A. P., and Liu, Y. Z. (2018). Preliminary experimental study of frost heaving pressure in crack and frost heaving propagation in rock mass under low temperature [J]. *Rock Soil Mech.* 39, 78–84. doi: 10.16285/j.rsm.2017.0059

Jang, J. G., Kim, H. K., Kim, T. S., Min, B. J., and Lee, H. K. (2014). Improved flexural fatigue resistance of PVA fiber-reinforced concrete subjected to freezing and thawing cycles. *Constr. Build. Mater.* 59, 129–135. doi: 10.1016/j.conbuildmat.2014.02.040

Jia, H., Xiang, W., and Krautblatter, M. (2015). Quantifying rock fatigue and decreasing compressive and tensile strength after repeated freeze-thaw cycles. *Permaf. Perig. Process.* 26, 368–377. doi: 10.1002/ppp.1857

Jia, H., Zi, F., Yang, G., Li, G. Y., Shen, Y., Sun, Q., et al. (2019). Influence of pore water (ice) content on the strength and deformability of frozen argillaceous siltstone. *Rock Mech. Rock Eng.* 1–18. doi: 10.1007/s00603-019-01943-0

Krautblatter, M., Funk, D., and Günzel, F. K. (2013). Why permafrost rocks become unstable: a rock-ice-mechanical model in time and space. *Earth Surf. Process. Landf.* 38, 876–887. doi: 10.1002/esp.3374

Krautblatter, M., Verleysdonk, S., Flores-Orozco, A., and Kemna, A. (2010). Temperature-calibrated imaging of seasonal changes in permafrost rock walls by quantitative electrical resistivity tomography (Zugspitze, German/Austrian Alps). *J. Geophys. Res.* 115, doi: 10.1029/2008JF001209

Lee, H., and Jeon, S. (2011). An experimental and numerical study of fracture coalescence in pre-cracked specimens under uniaxial compression. *Int. J. Solids Struc.* 48, 979–999. doi: 10.1016/j.ijsolstr.2010.12.001

Lei, B., Li, W., Tang, Z., Tam, V. W. Y., and Sun, Z. (2018). Durability of recycled aggregate concrete under coupling mechanical loading and freeze-thaw cycle in salt-solution. *Construc. Build. Mater.* 163, 840–849. doi: 10.1016/j.conbuildmat.2017.12.194

Li, Y. P., Chen, L. Z., and Wang, Y. H. (2005). Experimental research on pre-cracked marble under compression. *Int. J. Solids Struc.* 42, 2505–2516. doi: 10.1016/j.ijsolstr.2004.09.033

Lin, H., Yang, H., Wang, Y., Zhao, Y., and Cao, R. (2019). Determination of the stress field and crack initiation angle of an open flaw tip under uniaxial compression. *Theor. Appl. Fract. Mech.* 104:102358. doi: 10.1016/j.tafmec.2019.102358

Liu, C., Shi, B., Zhou, J., and Tang, C. (2011). Quantification and characterization of microporosity by image processing, geometric measurement and statistical methods: application on SEM images of clay materials. *Appl. Clay Sci.* 54, 97–106. doi: 10.1016/j.clay.2011.07.022

Liu, Q. S., Huang, S. B., Kang, Y. S., Pan, Y., and Cui, X. Z. (2015). Numerical and theoretical studies on frost heaving pressure in a single fracture of frozen rock mass under low temperature [J]. *Chin. J. Geotech. Engi.* 37, 1572–1580. doi: 10.11779/CJGE201509003

Liu, Y., Dai, F., Dong, L., Xu, N., and Feng, P. (2018). Experimental investigation on the fatigue mechanical properties of intermittently jointed rock models under cyclic uniaxial compression with different loading parameters. *Rock Mech. Rock Eng.* 51, 47–68. doi: 10.1007/s00603-017-1327-7

Matsuoka, N. (1995). A laboratory simulation on freezing expansion of a fractured rock: preliminary data. Ann. Rep. Instit. Geosci. 21. 5–8.

Matsuoka, N. (2008). Frost weathering and rockwall erosion in the southeastern Swiss Alps: long-term (1994-2006) observations. *Geomorphology* 99, 353–368. doi: 10.1016/j.geomorph.2007.11.013

Mu, Y., Ma, W., Li, G., Niu, F., Liu, Y., and Mao, Y. (2018). Impacts of supra-permafrost water ponding and drainage on a railway embankment in

continuous permafrost zone, the interior of the Qinghai-Tibet Plateau. *Cold Regions Sci. Technol.* 154, 23–31. doi: 10.1016/j.coldregions.2018.06.007

Murton, J. B., Peterson, R., and Ozouf, J. C. (2006). Bedrock fracture by ice segregation in cold regions. *Science* 314, 1127–1129. doi: 10.1126/science.1132127

Park, C. H., and Bobet, A. (2009). Crack coalescence in specimens with open and closed flaws: a comparison. *Int. J. Rock Mech. Min. Sci.* 46, 819–829. doi: 10.1016/j.ijrmms.2009.02.006

Park, C. H., and Bobet, A. (2010). Crack initiation, propagation and coalescence from frictional flaws in uniaxial compression. *Eng. Fract. Mech.* 77, 2727–2748. doi: 10.1016/j.engfracmech.2010.06.027

Pei, W., Zhang, M., Lai, Y., Yan, Z., and Li, S. (2019). Evaluation of the ground heat control capacity of a novel Air-L-shaped TPCT-ground (ALTG) cooling system in cold regions, *Energy* 179, 655–668 doi: 10.1016/j.energy.2019.04.156

Pudasaini, S. P., and Krautblatter, M. (2014). A two-phasemechanicalmodel for rock-ice avalanches. *J. Geophys. Res. F* 119, 2272–2290. doi: 10.1002/2014JF003183

Qiu, S. L., Feng, X. T., Zhang, C. Q., and Yang, J. B. (2012). Experimental research on mechanical properties of deep marble under different initial damage levels and unloading paths [J]. *Chin. J. Rock Mech. Eng.* 1, 1686–1697. doi: 10.3969/j.issn.1000-6915.2012.08.024

Rodríguez, P., Arab, P. B., and Celestino, T. B. (2016). Characterization of rock cracking patterns in diametral compression tests by acoustic emission and petrographic analysis. *Int. J. Rock Mech. Min. Sci.* 83, 73–85. doi: 10.1016/j.ijrmms.2015.12.017

Ruedrich, J., Kirchner, D., and Siegesmund, S. (2011). Physical weathering of building stones induced by freeze-thaw action: a laboratory long-term study. *Environ. Earth Sci.* 63, 1573–1586. doi: 10.1007/s12665-010-0826-6

Sahouryeh, E., Dyskin, A. V., and Germanovich, L. N. (2002). Crack growth under biaxial compression. *Eng. Fract. Mech.* 69, 2187–2198. doi: 10.1016/S0013-7944(02)00015-2

Shen, B., Stephansson, O., Einstein, H. H., and Ghahreman, B. (1995). Coalescence of fractures under shear stresses in experiments. *J. Geophys. Res.* 100, 5975–5990. doi: 10.1029/95JB00040

Shen, Y., Wang, Y., Yang, Y., Sun, Q., Luo, T., and Zhang, H. (2019). Influence of surface roughness and hydrophilicity on bonding strength of concrete-rock interface. *Construct. Build. Mater.* 213, 156–166. doi: 10.1016/j.conbuildmat.2019.04.078

Shen, Y. J., Yang, H. W., Xi, J. M., Yang, Y., Wang, Y. Z., and Wei, X. (2020). A novel shearing fracture morphology method to assess the influence of freeze–thaw actions on concrete–granite interface. *Cold Regions Sci. Technol.* 169:102900. doi: 10.1016/j.coldregions.2019.102900

Shen, Y. J., Zhang, Y. L., Gao, F., Yang, G. S., and Lai, X. P. (2018). Influence of temperature on the microstructure deterioration of sandstone. *Energies* 11:1753 doi: 10.3390/en11071753

Sun, W., Zhang, Y. M., Yan, H. D., and Mu, R. (1999). Damage and damage resistance of high strength concrete under the action of load and freeze-thaw cycles. *Cement Concrete Res.* 29, 1519–1523. doi: 10.1016/S0008-8846(99)00097-6

Tan, X., Chen, W., Liu, H., Wang, L., Ma, W., and Chan, A. H. C. (2018). A unified model for frost heave pressure in the rock with a penny-shaped fracture during freezing. *Cold Regions Sci. Technol.* 153, 1–9. doi: 10.1016/j.coldregions.2018.04.016

Tan, X., Chen, W., Yang, D., Liu, H., and Chan, A. H. C. (2019). Experimental and theoretical studies on effect of height-to-diameter ratios on failure forms and mechanical characteristics of foamed concrete. *J. Mater. Civil Eng.* 31:2557

Tan, X., Chen, W., Yang, J., and Cao, J. (2011). Laboratory investigations on the mechanical properties degradation of granite under freeze-thaw cycles. *Cold Regions Sci. Technol.* 68, 130–138. doi: 10.1016/j.coldregions.2011.05.007

Tang, C. A., Lin, P., Wong, R. H. C., and Chau, K. T. (2001). Analysis of crack coalescence in rock-like materials containing three flaws - Part II: numerical approach. *Int. J. Rock Mech. Min. Sci.* 38, 925–939 doi: 10.1016/s1365-1609(01)00065-x

Tutuncu, A. N., Podio, A. L., Gregory, A. R., and Sharma, M. M. (2002a). Nonlinear viscoelastic behavior of sedimentary rocks. Part I: effect of frequency and strain amplitude. *Geophysics* 63, 184–194. doi: 10.1190/1.1444311

Tutuncu, A. N., Podio, A. L., and Sharma, M. M. (2002b). Nonlinear viscoelastic behavior of sedimentary rocks, Part II: hysteresis effects and influence of type of fluid on elastic moduli. *Geophysics* 63, 195–203. doi: 10.1190/1.1444313

Walder, J., and Hallet, B. (1985). A theoretical model of the fracture of rock during freezing. *Geol. Soc. Am. Bull.* 96, 336–346. doi: 10.1130/0016-7606198596<336:ATMOTF<2.0.CO;2

Wang, S., Liu, Y., Du, K., and Zhou, J. (2019). Dynamic failure properties of sandstone under radial gradient stress and cyclical impact loading. *Front. Earth Sci.* 7:251. doi: 10.3389/feart.2019.00251

Wang, Y., Lin, H., Zhao, Y., Li, X., Guo, P., and Liu, Y. (2019). Analysis of fracturing characteristics of unconfined rock plate under edge-on impact loading. *Eur. J. Environ. Civil Eng.* doi: 10.1080/19648189.2018.1509021

Wong, L. N. Y., and Zhang, X. P. (2014). Size effects on cracking behavior of flaw-containing specimens under compressive loading. *Rock Mech. Rock Eng.* 47, 1921–1930. doi: 10.1007/s00603-013-0424-5

Wong, R. H. C., and Chau, K. T. (1998). Crack coalescence in a rock-like material containing two cracks. *Int. J. Rock Mech. Min. Sci.* 35, 147–164. doi: 10.1016/S0148-9062(97)00303-3

Xiao, J. Q., Ding, D. X., Jiang, F. L., and Xu, G. (2010). Fatigue damage variable and evolution of rock subjected to cyclic loading. *Int. J. Rock Mech. Min. Sci.* 47, 461–468. doi: 10.1016/j.ijrmms.2009.11.003

Xu, X., Li, Q., Lai, Y., Pang, W., and Zhang, R. (2019). Effect of moisture content on mechanical and damage behavior of frozen loess under triaxial condition along with different confining pressures. *Cold Regions Sci. Technol.* 157, 110–118. doi: 10.1016/j.coldregions.2018.10.004

Yang, G., Leung, A. K., Xu, N., Zhang, K., and Gao, K. (2019). Three-dimensional physical and numerical modelling of fracturing and deformation behaviour of mining-induced rock slopes. *Appl. Sci.* 9:1360. doi: 10.3390/app9071360

Yang, H., Liu, J., and Zhou, X. (2017). Effects of the loading and unloading conditions on the stress relaxation behavior of pre-cracked granite. *Rock Mech. Rock Eng.* 50, 1157–1169. doi: 10.1007/s00603-016-1161-3

Zhao, C., Niu, J., Zhang, Q., Yu, S., and Morita, C. (2019). Numerical simulations on cracking behavior of rock-like specimens with single flaws under conditions of uniaxial and biaxial compressions. *J. Mater. Civil Eng.* 31:04019305. doi: 10.1061/(asce)mt.1943-5533.0002967

Zhao, Y., Wang, Y., Wang, W., Tang, L., Liu, Q., and Cheng, G. (2019). Modeling of rheological fracture behavior of rock cracks subjected to hydraulic pressure and far field stresses. *Theor. Appl. Fract. Mech.* 101, 59–66. doi: 10.1016/j.tafmec.2019.01.026

Zhou, X. P., Cheng, H., and Feng, Y. F. (2014). An experimental study of crack coalescence behaviour in rock-like materials containing multiple flaws under uniaxial compression. *Rock Mech. Rock Eng.* 47, 1961–1986. doi: 10.1007/s00603-013-0511-7

Conflict of Interest: The authors declare that the research was conducted in the absence of any commercial or financial relationships that could be construed as a potential conflict of interest.

Copyright © 2019 Shen, Yang, Jin, Zhang, Yang and Zhang. This is an open-access article distributed under the terms of the Creative Commons Attribution License (CC BY). The use, distribution or reproduction in other forums is permitted, provided the original author(s) and the copyright owner(s) are credited and that the original publication in this journal is cited, in accordance with accepted academic practice. No use, distribution or reproduction is permitted which does not comply with these terms.